RESULTS OF BUOYANCY-GRAVITY EFFECTS IN ITER CABLE-IN- CONDUIT CONDUCTOR WITH DUAL CHANNEL

P. Bruzzone[1], B. Stepanov[1], R. Zanino[2], L. Savoldi Richard[2]

[1]EPFL - CRPP – Technologie de la Fusion
5232 Villigen-PSI, Switzerland

[2]Dip. di Energetica, Politecnico,
24, corso Duca degli Abruzzi, 10129 Torino, Italy

ABSTRACT

The coolant in the ITER cable-in-conduit conductors (CICC) flows at significant higher speed in the central channel than in the strand bundle region due to the large difference of hydraulic impedance. When energy is deposited in the bundle region, e.g. by ac loss or radiation, the heat removal in vertically oriented dual channel CICC with the coolant flowing downward is affected by the reduced density of helium (buoyancy) in the bundle region, which is arising from the temperature gradient due to poor heat exchange between the two channels. At large deposited power, flow stagnation and back-flow can cause in the strand bundle area a slow temperature runaway eventually leading to quench.

A new test campaign of the thermal-hydraulic behavior was carried out in the SULTAN facility on an instrumented section of the ITER Poloidal Field Conductor Insert (PFIS). The buoyancy-gravity effect was investigated using ac loss heating, with ac loss in the cable calibrated in separate runs. The extent of upstream temperature increase was explored over a broad range of mass flow rate and deposited power. The experimental behavior is partly reproduced by numerical simulations. The results from the tests are extrapolated to the likely operating conditions of the ITER Toroidal Field conductor with the inboard leg cooled from top to bottom and heat deposited by nuclear radiation from the burning plasma.

KEYWORDS: Cable-in-conduit, Dual channel, Thermo-hydraulic behavior.
PACS: 47.20.Bp, 44.27.+g, 84.71.Fk

CP823, *Advances in Cryogenic Engineering: Transactions of the Cryogenic Engineering Conference - CEC, Vol. 51,* edited by J. G. Weisend II

INTRODUCTION

In the early conceptual design of dual channel cable-in-conduit conductors [1], it was assumed that temperature and pressure are uniform over the conductor cross section. Actually, the coolant speed is much higher in the central channel and acts as a pressure release in case of a quench. The coolant also provides an improvement in the heat removal due to the shorter, average residence time in the winding.

A two-fluid model, with distinct temperature and pressure in the two channels, was proposed in [2]. Later experiments [3] brought evidence of large temperature gradients within the bundle area, persisting over long length, and induced a multi-channel / multi-fluid model. The issue of the heat transfer between the central hole and the bundle area was first discussed by A. Long [4]. Recent tests in SULTAN allowed a quantitative assessment of the "global" heat exchange between central hole and bundle area [5-6].

THE BUOYANCY-GRAVITY EFFECT

The buoyancy induced flow motion is a direct consequence of the slow temperature homogenization (poor heat exchange) over the CICC cross section. When the conductor is vertically oriented, a heat deposition in the strand bundle area establishes a temperature and density gradient between the central channel and the bundle area. Depending on the flow direction, either top-to-bottom or bottom-to-top, the buoyancy due to the lower density in the strand bundle causes either a deceleration or an acceleration of the coolant flow in the bundle, respectively.

In the case of top-to-bottom flow, increasing power deposition in the strand bundle causes the flow velocity to be reduced until the buoyancy balances the pressure drop (coolant stagnation). Eventually, the flow reverses in the bundle area inducing a thermo-siphon loop, FIGURE 1.

Once the thermo-siphon loop is established, the local heat removal from the bundle area is very poor and a local temperature runaway due to heat accumulation may occur even at moderate power deposition, i.e. at moderate temperature increase of the overall mass flow rate

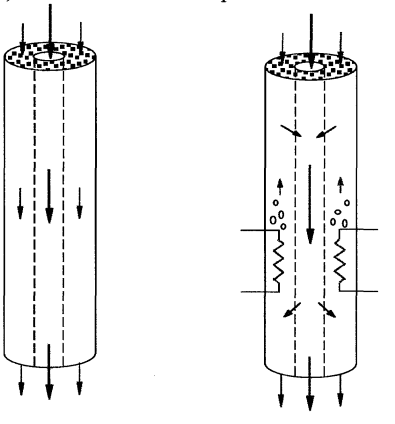

FIGURE 1. Schematic representation of the buoyancy-gravity effect in a dual channel CICC with coolant flow top-to-bottom and heat deposited in the bundle area

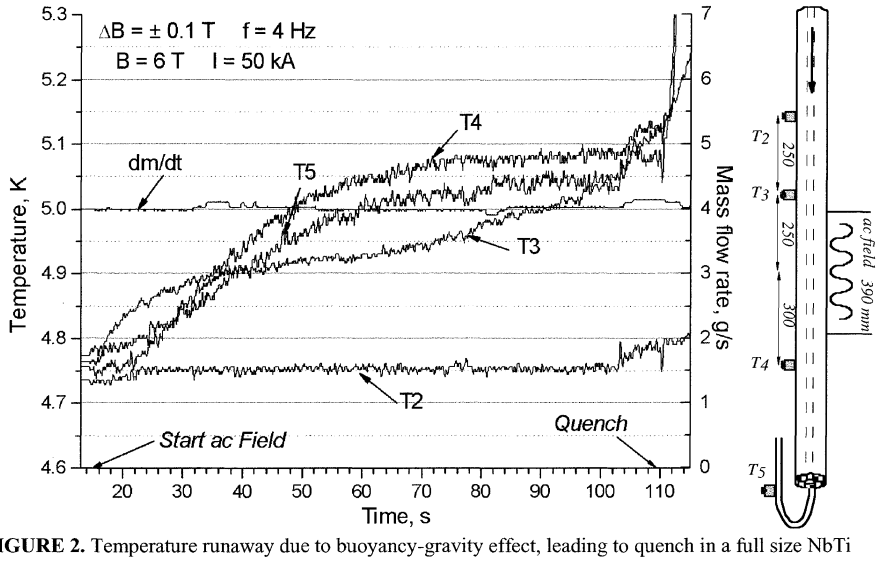

FIGURE 2. Temperature runaway due to buoyancy-gravity effect, leading to quench in a full size NbTi sample (PF-FSJS, September 2002). The sensor location is depicted in the sketch at the right end side

at the outlet of the CICC.

The first experimental evidence of the potential catastrophic consequence of the buoyancy-gravity effect was observed in a NbTi CICC full size SULTAN sample in September 2002 [7]. A sketch of the sample instrumentation and the relevant plot of the experimental run are shown in FIGURE 2. In the background field of 6 T, operating current 50 kA and operating temperature 4.7 K, the temperature margin, measured on dc runs, is 1.2 K. With a superimposed ac field of $\Delta B = \pm 0.1$ T and f = 4 Hz, the ac loss power, separately measured during another run, is in the range of 4 W. This causes a temperature increase of ≈ 0.25 K at an overall mass flow rate (bundle + central channel) of 4 g/s, as this is observed at the T5 sensor. However, during a run with long ac field sweep, it is observed that the overall mass flow rate is constant but the temperature T3 upstream of the ac field does increase, which proves the flow stagnation/reversal in the bundle region. After about two minutes of local heat accumulation in the bundle region, the conductor quenches although the outlet temperature (T5) is still about 1 K below T_{cs}.

S. Nicollet [8] first brought a consistent interpretation of the effect in January 2003 and the experimental results were partly reproduced by a numerical model [9].

RESULTS OF THE PF INSERT CONDUCTOR SAMPLE IN SULTAN

A sample of the ITER Poloidal Field Insert Conductor (PFIS) was tested in SULTAN in 2004 [10]. After the main test campaigns in March – May 2004, the sample was modified reversing the coolant flow direction and removing the electrical connections (to avoid heat exchange between the two conductors at the joint). In September 2004, the sample was assembled again for a thermo-hydraulic test in SULTAN.

TABLE 1. Layout of the two full size NbTi CICC's of the PFIS.

	L (with subcable wraps)	**R** (without wraps)
NbTi Strand Diameter, mm	0.73	
Number of strands / cosθ	1440 / 0.96	
Steel spiral for central channel, mm	10 x 12	
Spiral gap, mm / perforation, %	≈1.7 / ≈ 20	
Cable space diameter, mm	37.53	36.89
Void fraction in the bundle area, %	33.5	34.3
Retained hydraulic diameter in bundle area, mm	0.412	0.454
Outer wraps cross section, mm^2	≈ 22	-
Subcable wraps cross section, mm^2	≈ 13	-
Subcable wraps coverage, %	80	-

The PFIS consists of two conductor sections, one with subcable wraps (label L) and the other without (label R). The relevant conductor data for the thermo-hydraulic tests are gathered in TABLE 1. More details on the conductor layout are in [10]. The friction factor results from room temperature tests with pressurized water are discussed in [11].

The most effective way to deposit heat homogeneously in the bundle area is by ac loss. Both conductor sections are tested separately for ac loss, with upward flow direction. The power loss is measured by gas flow calorimetry vs. the frequency of the applied field, using sensors placed in the outlet pipe, i.e. collecting the flow of both the central channel and the bundle area. The results, similar for the two conductors, are shown in FIGURE 3, for the range 0.2 – 4 Hz. The power is deposited over about 390 mm length. A 3rd order polynomial, is used to interpolate the loss at any frequency within the test range.

For the investigation of the buoyancy-gravity effect, the heat was deposited either by ac loss or by a 10 mm long annular heater glued on the machined jacket (wall thickness about 2 mm). The mass flow rate (from top to bottom) was set at 2, 4, 6 and 8 g/s. The location of

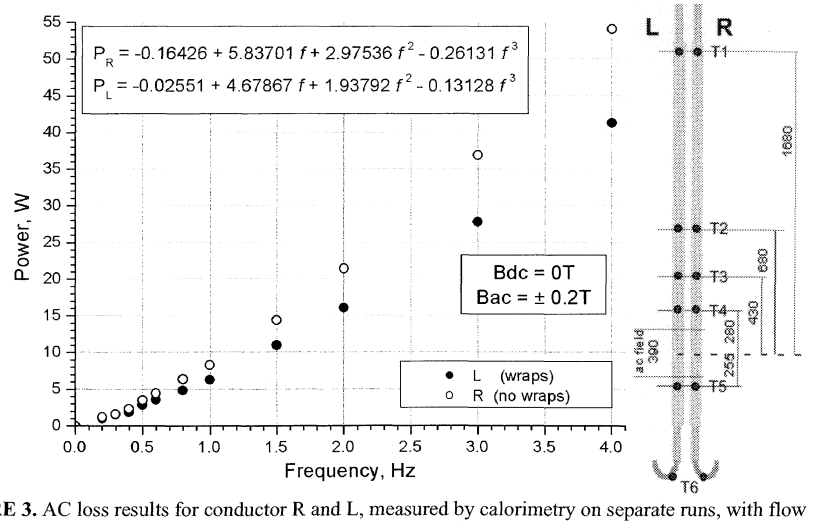

FIGURE 3. AC loss results for conductor R and L, measured by calorimetry on separate runs, with flow direction bottom-to-top. To the right, instrumentation scheme for the thermal-hydraulic tests

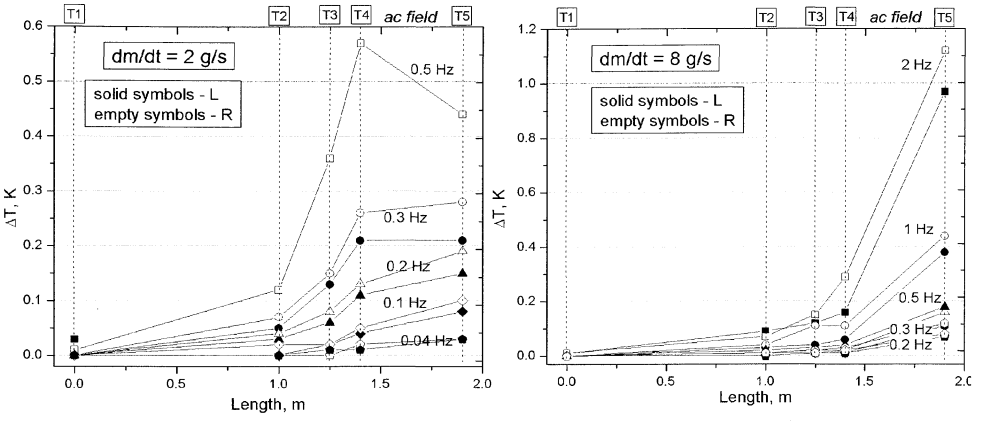

FIGURE 4. Summary of ΔT profiles along the two conductors for ac loss heating with mass flow rate 2 g/s (left plot) and 8 g/s (right plot).

the five temperature sensors (T1 to T5) attached to the jacket of both conductors is shown in the sketch on the right side of FIGURE 3.

The temperature increase, ΔT, as recorded by the sensors is shown in FIGURES 4 and 5 after about 2-3 minutes of ac field sweep. Before the ac field sweep, the absolute temperature read-out is not the same along the conductor [12], This is unexpected because of the almost negligible difference between inlet and outlet temperature as measured by the facility sensors. The discrepancy may be due to non-proper thermal anchoring (heat sink) of the sensor leads to the conductor jacket. For the comparison with the simulation using the 1D codes, the readout of the temperature sensors (including ΔT) has been re-scaled to represent the average temperature over the bundle area. Results from heat steps runs devoted to calibration were used to this purpose.

The plots in FIGURE 4 report the steady state ΔT profiles along the conductors for different frequencies (i.e. power) of the ac field. For a non-perturbed flow, the temperature profile upstream of the ac field should stay flat, i.e. ΔT = 0.

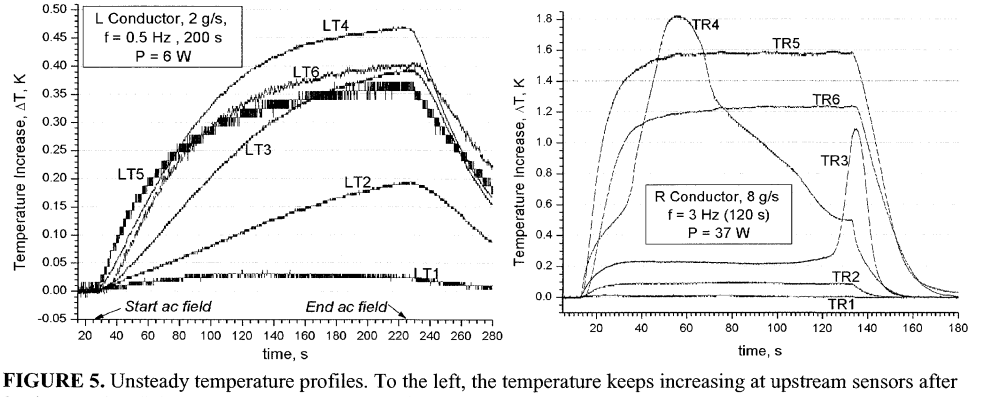

FIGURE 5. Unsteady temperature profiles. To the left, the temperature keeps increasing at upstream sensors after 3 minutes of ac field sweep. To the right, unstable profile at high power, high mass flow rate

At low mass flow rate, flow stagnation and reversal occurs at lower deposited power because the pressure drop to be overcome is smaller and the buoyancy is higher due to the lower heat removal rate. At higher mass flow rate, the perturbations upstream of the ac field are smaller but still observable even at very low power deposition.

In some cases, no steady state temperature profile is achieved during the experimental run. In FIGURE 5, left, the temperature evolution is shown for the L conductor at 2 g/s, 0.5 Hz. The upstream temperature (T4 and T3) keeps increasing well above the level of T5 (jacket downstream) and T6 (outlet pipe) even after 200 seconds of ac field sweep (full flow reversal). On the right side of FIGURE 5, flow instabilities with large temperature jumps at the upstream sensors are observed starting at 3 Hz ac field (over 30 W) at 8 g/s. In both cases, local heat accumulation occurs in the strand bundle eroding the temperature margin and likely leading to a quench in actual operation, with non-zero operating current.

NUMERICAL SIMULATION

In the cases where no instabilities appear, it was possible to reproduce numerically the experimental results using the Mithrandir code [2]. The shot selected for the simulations are presented in FIGURE 5 left (2 g/s, ac pulse @ 0.5 Hz for 200s). In the simulations, constant mass flow rate, inlet temperature and outlet pressure were assumed as boundary conditions and the power was assumed to be a square wave in space and time fully deposited in the cable region (no power in the jacket). The use of the friction factors as in [11] guaranteed the correct computation of the initial flow repartition, which is a crucial issue and a new ingredient with respect to the previous analysis of the PF-FSJS [9]. The heat transfer coefficient between hole and bundle were assumed constant and equal to 150-200 W/m^2K (deduced from other thermal-hydraulic tests of the PFIS), which is also a new ingredient of the analysis. The effective perforated fraction of the interface between hole and bundle was assumed ad-hoc to be much smaller (0.002 for the left leg, with wraps, 0.005 for the right leg) than the nominal one (0.2) because of our ignorance on the advection mechanism between the two regions. The computed results in FIGURE 6 for the left leg and right leg, respectively, show a very good quantitative agreement with the experimental temperatures (corrected as discussed above) for both legs.

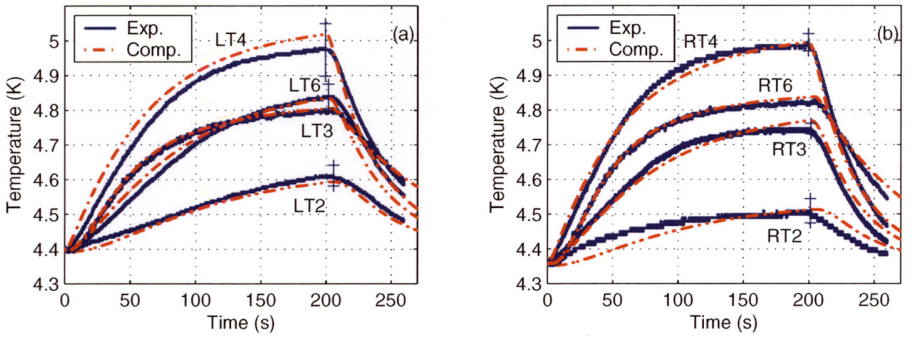

FIGURE 6. AC run at 0.5 Hz, 200s, with mass flow rate of 2 g/s. Evolution of the re-scaled, experimental (solid) and computed (dash-dotted) temperatures at different sensors along the left leg (a) and right leg (b), respectively. The error bars of the correction of the experimental signals are also reported for completeness.

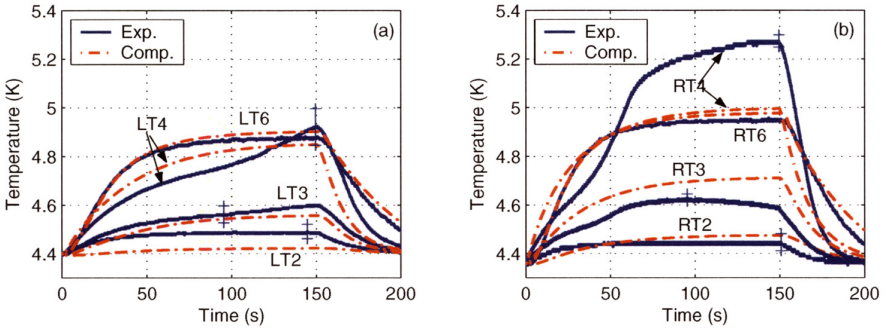

FIGURE 7. AC run at 1 Hz, 150s, with mass flow rate of 4 g/s. Evolution of the re-scaled, experimental (solid) and computed (dash-dotted) temperatures at different sensors along the left leg (a) and right leg (b), respectively. The error bars of the correction of the experimental signals are also reported for completeness.

The capability of the code to reproduce quantitatively the experimental results deteriorates when instability appears, as it is shown in FIGURE 7, for a run with ac field at 1 Hz, 4 g/s. The computed results have been obtained with frozen coupling parameters between hole and bundle. For the left leg (FIGURE 7a), computation and experiment still reasonably agree with the exception of LT4, for which the change of slope is not captured. For the right leg (FIGURE 7b) the buoyancy effect is underestimated at T4 but overestimated at T3 and T2, possibly indicating that a more refined coupling model between the bundle and hole region (correlation for the heat transfer coefficient as well as improved model of the advective processes) is required to capture the very details of "unstable" cases.

The ITER inboard leg

In the first turn of the ITER TF coil inboard leg, about 8 m long, with flow top-to-bottom, the expected nuclear heat radiation is 7.5 / 10.5 W per conductor for the scenarios of 500/700 MW plasma. The nominal mass flow rate is 8 g/s. In a conductor like PFIS, these conditions would produce a moderate buoyancy gravity effect, see FIGURE 4 right, with an upstream temperature increase of ≈ 0.2 K.

Compared to PFIS, the TF conductor has a smaller spiral (7x9 mm vs. 10x12 mm) and a larger flow area in the annular region (406 mm^2 vs. 333 mm^2). The length for heat deposition is also longer ($\approx$ 8 m vs. 0.4 m). For the above reasons, the power deposition threshold for relevant buoyancy-gravity effects is expected to be higher for TF conductor than for PFIS, although the effect of parallel flow channels with total imposed mass flow rate (as opposed to the PFIS case and analysis) still has to be investigated.

CONCLUSION

Evidence of flow perturbations (temperature increase upstream of the heat generation) in dual channel CICC, even at low power deposition, due to buoyancy-gravity effects was observed during dedicated tests of the PFIS sample in SULTAN.

Numerical simulations show that for low input power the available 1D codes are able to reproduce the buoyancy effects with a very good accuracy once the thermal-hydraulic characterization of the conductor is available (friction factors and heat transfer coefficients from dedicated tests) and an ad-hoc perforated fraction is retained. The capability of the code to accurately reproduce the measured temperatures reduces when instabilities onset in the experiments.

Based on the PFIS tests, the condition for flow reversal and large heat accumulation in the vertical, straight leg of the ITER TF coils are presumably not fulfilled at the nominal mass flow rate. The implication of the buoyancy-gravity effect may result in a marginal reduction of operating margin, which has to be carefully watched due to the risk of runaway effect in connection with the rapidly increasing index loss (an n index as low as 7 is retained presently in the ITER Nb_3Sn cable design). A thermal-hydraulic test of the actual ITER TF conductor (smaller central channel and void fraction compared to PFIS) is recommended for a final assessment.

ACKNOWLEDGMENT

EFDA partly supported this work. The work of RZ and LSR was also supported by MIUR. The authors are indebted to M. Vogel, R. Dettwiler, F. Roth and F. Stähli for support and technical assistance. The technical support of the Paul Scherrer Institute (PSI) is greatly acknowledged.

REFERENCES

1. Luongo C.A., Chang C.L., Partain K.D., "A computational quench model applicable to the SMES/CICC", *IEEE Trans. Mag.* **30**, pp 2569-2572 (1994)
2. Zanino R., De Palo S., Bottura L., "A Two-Fluid Code for the Thermohydraulic Transient Analysis of CICC Superconducting magnets", *J. Fus. Energy*, **14** (1), pp 25-40 (1995)
3. Bruzzone P., Fuchs A.M., Vecsey G., Zapretilina E., "Test Results for the high field Conductor of the ITER Central Solenoid Model Coil", *Adv. Cryog. Eng.*, **45 A**, pp 729-736 (2000)
4. Long A.L., Master of Science in Mechanical Engineering, MIT, Cambridge, MA, 1995
5. Renard B., Duchateau J-L., "Transient and steady state measurement of dual channel CICC heat transef coefficients on a full size ITER conductor", presentation at CHATS 2005, submitted to *Cryogenics*
6. Bottura L., Bruzzone P., Marinucci C., Stepanov B., "Transverse Heat Transfer Coefficient in CICC's with Central Cooling Channel", paper C2-L-02 at CEC 2005, Keystone
7. Bruzzone P., "Learning about hydraulic and stability through an ac loss test", Unpublished presentation at CHATS 2002, Karlsruhe, September 2002
8. Nicollet S., Ciazynski D., "Thermohydraulics & calibrations", Unpublished presentation at CRPP Workshop, Gstaad January 2003
9. Zanino R., Bruzzone P., Ciazynski D., Ciotti M., Gislon P., Nicollet S., Savoldi Richard L., "Analysis of Thermal-Hydraulic Effects in the Testing of the ITER Poloidal Field Full Size Joint Sample (PF-FSJS)", *Adv. Cryog. Eng.* **49 A**, pp 544-551 (2004)
10. Bruzzone P. et al., "Test Results of the ITER PF Insert Conductor short Sample in SULTAN", *IEEE Trans Appl. Supercon.* **15**, pp 1351-1354 (2005)
11. Marinucci C., CRPP Internal Report/SC/2005/CM01, June 2005
12. Bruzzone P., memo#26 to the PFIS Testing Group, CRPP September 2004